POLITECNICO DI TORINO
Repository ISTITUZIONALE

Targeting the high frequency tail of wave spectra for energy harvesting in marine sensor networks

Original
Targeting the high frequency tail of wave spectra for energy harvesting in marine sensor networks / Davidson, J., Nava, V.. - In: RENEWABLE ENERGY. - ISSN 0960-1481. - 237:(2024). [10.1016/j.renene.2024.121550]

Availability:
This version is available at: 11583/2995587 since: 2024-12-18T14:22:51Z

Publisher:
Elsevier Ltd

Published
DOI:10.1016/j.renene.2024.121550

Terms of use:

This article is made available under terms and conditions as specified in the corresponding bibliographic description in the repository

Publisher copyright
Elsevier postprint/Author's Accepted Manuscript

© 2024. This manuscript version is made available under the CC-BY-NC-ND 4.0 license
http://creativecommons.org/licenses/by-nc-nd/4.0/.The final authenticated version is available online at:
http://dx.doi.org/10.1016/j.renene.2024.121550

(Article begins on next page)

15 November 2026

Targeting the high frequency tail of wave spectra for energy harvesting in marine sensor networks

Josh Davidson[a,*], Vincenzo Nava[a,b]

[a] *Basque Center for Applied Mathematics, Mazarredo 14, 48009 Bilbao, Spain*
[b] *TECNALIA, Basque Research and Technology Alliance (BRTA), Derio, Bizkaia, Bilbao, Spain*

Abstract

While the conventional philosophy of wave energy conversion is to target the large amounts of power in the peak of the input wave spectrum, this study proposes that for the application of powering marine sensor networks (MSNs), it is advantageous to target the high frequency tail of the wave spectrum. This strategy is predicated on two primary advantages: the spatial and temporal persistence of the wave energy resource in the high-frequency region and its compatibility with the resonance characteristics of smaller MSN devices. The research seeks to identify the frequency range in sea spectra which is temporally and spatially omnipresent in the marine environment, and quantify the energy content available within this range. Theoretical frameworks are combined with a detailed case study to analyse the temporal and spatial variations of the wave resource and the persistent energy content in the high-frequency tail. Results reveal a notable consistency in energy availability above 2.5 rad/s, highlighting the high-frequency tail's potential as a reliable energy resource for MSNs. The available power in the identified high-frequency range is quantified, providing valuable insights for the design and implementation of efficient wave energy harvesters specifically tailored to the needs of diverse marine environments.

Keywords: Wave energy, Energy Harvesting, Wave Resource Analysis, Marine Renewable Energy, Autonomous Wireless Sensors, Environmental Monitoring, Ambient Energy Scavenging, TENGs

1. Introduction

The emergence of wireless sensor networks (WSNs) and the Internet of Things has revolutionised the monitoring of marine environments, enabling both remote and near real-time observation. These innovative sensor networks are deployed across a multitude of coastal and ocean settings, bringing about a paradigm shift in environmental monitoring and management through unparalleled data collection and analytical capabilities. However, the broader implementation of these Marine Sensor Networks (MSNs) faces a significant challenge – the critical issue of power supply. This paper aims to address this challenge, exploring the potential of wave energy harvesting from the high frequency part of the wave spectrum to provide a robust renewable energy source for MSNs.

*Corresponding author.
Email address: jdavidson@bcamath.org (Josh Davidson)

Electronic copy available at: https://ssrn.com/abstract=4758518

1.1. Marine Sensor Networks

First proposed by Curtin et al. [1] in the 1990s, the concept of autonomous oceanographic sampling networks was born from the need to measure oceanic temporal and spatial gradients beyond current capabilities. Rajasegarar et al. [2] highlighted these challenges in the context of the Great Barrier Reef, underscoring the limitations of traditional data logging systems in capturing dynamic environmental data. The integration of WSNs into the monitoring of coastal and ocean regions heralds a significant advancement, enabling data collection at unprecedented spatial and temporal resolutions. This enhancement not only elevates the quality of information gathered but also facilitates its near real-time accessibility, thereby greatly augmenting its value for a diverse range of stakeholders including researchers, policymakers, and environmental managers.

Early developments in MSNs, notably the SEMAT project [3–6], focused on advanced WSNs for environmental research, including climate change, water quality, and ecosystem health. Industrial applications also fueled MSN development, for example as seen in the OceanSense project [7], which originated from a need to monitor silt deposition in a major Chinese coal transportation harbor [8]. By deploying WSNs for sea depth monitoring, OceanSense achieved a significant reduction in monitoring costs by 95%. These studies laid the groundwork for the wide array of applications now encompassed by MSNs. These include temperature monitoring in cold water upwelling zones [9], marine environment data collection [10], ship detection systems [11], high-resolution wave monitoring [12], early warning systems for tsunamis and coastal freak waves [13], drifting WSNs for oil spill monitoring [14], and aquaculture applications such as monitoring the amount of uneaten food and fecal waste by the fish [15] and aquatic environment monitoring for marine shellfish breeding [16]. MSNs have been effectively used in windfarm studies for examining sedimentation and wave processes in relation to wind turbine installations [17] and have been integrated into larger systems like the Coastal Ocean Observation System of Murcia Region [18]. For a more in-depth coverage of the diverse range of MSN applications, the reader is referred to the comprehensive reviews by Albaladejo et al. [19], Xu et al. [20], and Mishra et al. [21], which illustrate the evolution and growing importance of MSNs.

Despite these advancements, the widespread deployment of MSNs is hampered by the fundamental issue of power supply. The remoteness of these networks renders traditional power sources like batteries impractical, exacerbated by the high energy demands of long-range data transmission and signal attenuation in the constantly moving sea environment [19, 22]. This predicament highlights the urgent need for reliable energy harvesting methods for MSNs from a renewable energy source.

Electronic copy available at: https://ssrn.com/abstract=4758518

1.2. Wave Energy Harvesting for Marine Sensor Networks

The concept of energy harvesting for WSNs [23, 24], is highly relevant for MSNs. An overview of energy harvesting possibilities specifically for marine-based sensors is provided in [25], with wave energy emerging as the strongest candidate renewable energy source. The attraction towards ocean waves as a renewable energy source lies in their considerable and consistent power flux, a feature that surpasses other sources like wind and solar energy. Pelc and Fujita [26] underscore this reliability, noting that wave power is typically available up to 90% of the time at specific sites, in contrast to the 20-30% availability of solar and wind power. The limited efficiency of solar cells during certain seasons, particularly in high latitudes, was observed in a Baltic Sea MSN for water temperature measurement [27], leading to the authors suggesting the combined usage of wave and solar energy harvesters.

The application of wave energy harvesting for MSNs introduces unique challenges and design requirements that differ significantly from those of conventional large-scale wave energy converters (WECs). MSN-oriented wave energy harvesters must be small, cheap, structurally simple and easily deployable [25, 28, 29]. In contrast to large-scale WECs, which are typically installed at sites with optimal wave conditions, the deployment locations of MSN wave energy harvesters are dictated by the MSN monitoring objectives rather than the wave resources, ranging from sheltered areas to open waters and in some cases freely drifting across multiple locations [30]. Therefore, these MSN wave energy harvesters require a versatile 'one size fits all' design approach, allowing for cost reduction through mass production and reusability, as opposed to custom designs tailored to a specific site. Albaladejo et al. [31] highlight 'low cost' and 'ease of deployment' as key advantages of their sensor-buoy design, which emphasises the importance of cost-effectiveness and simplicity in the design and deployment of MSN wave energy harvesters. Ideally, these devices should be compact enough to allow single-person deployment from any standard vessel, eliminating the need for specialised equipment or personnel.

The potential of wave powered sensor buoys is evidenced by the recent surge of activity in this field. Detailed literature reviews on wave powered sensor buoys are available for the interested reader in recent publications [28, 32, 33], which shed light on the evolving landscape of wave energy harvesting. These reviews highlight the progress in the field and the continuous efforts to adapt and optimise WECs for diverse marine conditions. This is particularly important for MSNs, where the specific demands and challenges require efficient and sustainable power solutions.

1.3. Targetting the high frequency tail of wave spectra

This paper proposes that the high frequency tail of wave spectra is an attractive resource due to two primary factors: the nature of the wave resource and the dynamics of small-scale devices.

The wave field generation is influenced by wind speed, duration, and fetch length, leading to diverse wave spectra at a single site and also a wide variety between sites. However, Phillips [34] noted that, "...for low frequencies, the spectrum curves depend quite strongly on the fetch and

Electronic copy available at: https://ssrn.com/abstract=4758518

the meteorological conditions, but their most remarkable property is that for high frequencies, the curves obtained under different conditions very nearly coincide and become apparently independent of the fetch and of the strength of the wind." The high frequency part of the spectrum is first part to be created when the wind blows and forms a similar shaped spectrum independent on the fetch and wind speed, as illustrated in Figure 1(a) which compares the JONSWAP spectrum [35] for locations with various fetch lengths.

This consistency in spectrum shape is a very attractive feature of the high frequency region, allowing a wave energy harvester to be designed for this input condition, with confidence that it will be persistent irrespective of location or time. An additional potential benefit, particular for coastal locations, is that in nearshore areas there is often a second spectral peak at twice the frequency of the main wave, linked to the asymmetrical shape of shallow water waves, as depicted in Figure 1(b). This energy transfer from low to high frequencies as swell waves propagate into coastal regions, possibly enhances the energy resource in the high frequency tail for powering MSNs.

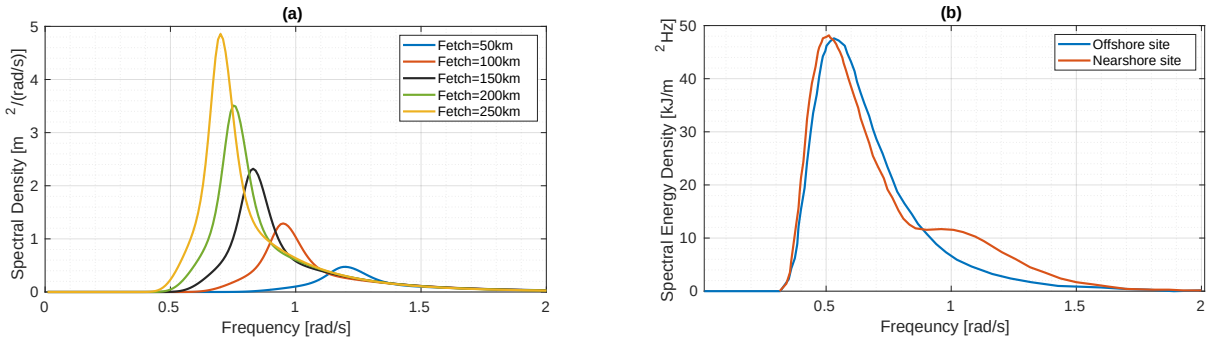


Figure 1. (a)Example of the change in spectral shape with fetch length for a JONSWAP spectrum (12m/s wind speed) (b) Example of the change in spectral shape with water depth (From [36]).

The second key reason for targeting the high frequency tail of wave spectra in MSNs is its compatibility with the natural dynamics of small-scale devices. Small-scale devices are generally not well-suited to low-frequency operation as they tend to have high-frequency natural responses. This makes the high-frequency portion of the wave spectrum particularly advantageous for creating efficient, small-sized wave energy harvesters.

For example, the resonant frequency of the water column in a heaving Oscillating Water Column (OWC), which has been proposed as a power source for sensor buoys [29, 37] and traces its roots back to Masuda's pioneering work on OWC powered navigational buoys in the 1940s [38]. The natural frequency of a water column with a constant cross-section, such as a pipe, is given by $\omega_{0,OWC} = \sqrt{\frac{g}{L}}$, where L is its length and g is the gravitational acceleration. As illustrated in Figure 2(a), for an OWC to resonate with waves below 1 rad/s, the pipe length must exceed 10 meters.

A second illustration is the hydrodynamic natural frequency of a heaving sphere. To resonate below 1 rad/s, a sphere would need a diameter exceeding 20 meters. Figure 2(b) shows the response amplitude operator (RAO) for heaving spheres of various radii, with resonant peaks for spheres

Electronic copy available at: https://ssrn.com/abstract=4758518

under 1 meter in diameter exceeding 4 rad/s. Comparing these RAOs with corresponding velocity transfer functions, as shown in Figure 2(c), underscores another benefit of high-frequency operation: higher velocities for the same displacement amplitude. Since the power output from vibration energy harvesters is proportional to the velocity squared, operating at higher frequencies can generate more power within a given displacement limit.

This principle also applies to non-resonant PTO devices such as Triboelectric Nanogenerators (TENGs), where higher frequency operation is beneficial. As identified in the wave energy harvesting reviews [28, 33, 39] TENGS are a very hot area of research and has its own dedicated review in [40]. TENG systems, which function through contact and separation or sliding movements between two tribo-materials, demonstrate that higher frequency input waves lead to increased power output [41, 42]. Research on TENGs typically considers waves in the 1 - 3Hz range, termed "low frequency" in the context of nanotechnology and vibration energy harvesting, but this range actually falls into the high-frequency tail region for ocean waves. The review by Rodrigues et al. [40] details TENG prototypes for wave energy harvesting in buoys: 6 of these studies considered frequencies between 5 and 10 rad/s [43–48] and the remaining 9 considered frequencies above that up to 25 rad/s [49–56].

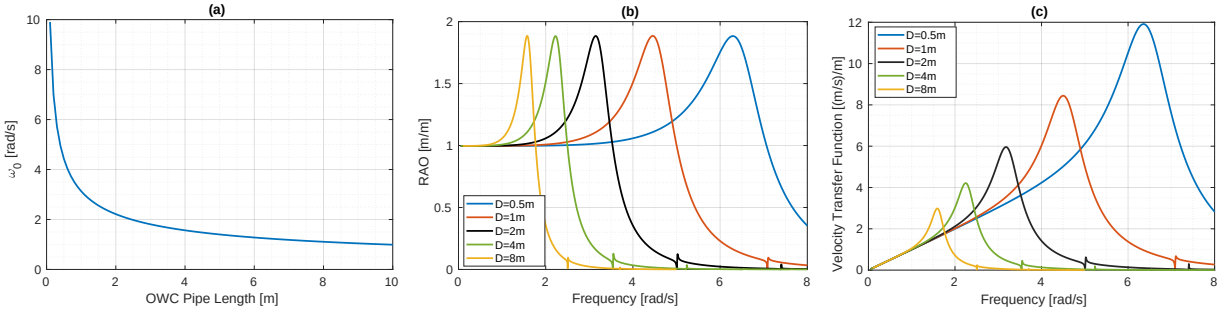


Figure 2. (a) Natural frequency of a OWC as a function of its length, (b) RAO of a heaving sphere for various diameters, and (c) The velocity transfer function for the same heaving spheres.

1.4. Objective and outline of paper

This paper introduces a novel wave energy harvesting approach, focusing on the high frequency tail of the wave spectrum. Diverging from traditional research that targets lower frequency, more powerful waves, this study highlights the unique benefits of high frequency waves for powering small-scale marine equipment. Combining theoretical analysis with real-world case studies, it aims to identify consistently present wave spectrum segments and quantify their accessible power.

To achieve this goal, the paper is laid out as follows: Section 2 delves into a theoretical examination of the high frequency tail of ocean wave spectra, laying the foundational understanding for subsequent analyses. In Section 3, the paper presents a study of 12 diverse sites, focusing on their wave climates and spectra to offer a broad perspective on varying wave resources. The insights and data garnered from both the theoretical and empirical studies are then synthesised in Section 4, where the implications and significance of the findings are discussed. Finally, Section 5 encapsulates the key conclusions drawn from the study.

Electronic copy available at: https://ssrn.com/abstract=4758518

2. Theoretical investigation

Wave spectra, represented as $S(\omega)$, are critical in depicting the frequency domain representation of surface elevation variance at a point. These spectra are derived from measured time series and provide valuable insights into the energy distribution across different wave frequencies. The investigation here aims to dissect and understand the high frequency portion of these wave spectra.

2.1. The form of the high frequency tail

The consistency in the shape of the high frequency part of all wave spectra was first identified by Burling [57], who found empirically that the mean values of his observed spectra at high frequency obeyed a relation of this type:

$$S_B(\omega) = 0.7\omega^{-5}. \tag{1}$$

Using dimensional analysis Phillips [34] derived the following expression for the high frequency components of the wave spectrum:

$$S_P(\omega) = \alpha g^2 \omega^{-5}, \tag{2}$$

which for an α value of 7.4×10^{-3} agrees with Burling's measurements. This is also consistent with the Pierson-Moskowitz (PM) [58] and JONSWAP spectra [35] for high frequencies, where an α value of 8.1×10^{-3} is used. Figure 3 plots a comparison of the PM spectrum for varying windspeeds against Burling's curve, Eqn 1, showing that the convergence of the PM spectrum to Burling's curve at high frequencies.

Subsequent studies have suggested that this part of the spectrum is better fit with an ω^{-4} relationship. Toba [59] first proposed the ω^{-4} form for the high frequencies of ocean wave spectra in the gravity wave range, using data from wind-wave tunnel experiments, and then results from subsequent field experiments presented in [60] supported this form. Specifically, Toba [59] empirically derived the following expression for the high frequency side of the spectrum:

$$S_T(\omega) = \alpha_T g u^* \omega^{-4}. \tag{3}$$

where u^* is the friction velocity and α_T was determined to be 0.02 for the wind-wave tunnel experiments and 0.062 from the field experiments. Kahma [61] studied the development of the wave spectrum with fetch in a steady wind using a line of consecutive wave buoys in the Bothnian Sea. In the saturation range the spectrum was found to have the form:

$$S_K(\omega) = \alpha_K U_{10} g \omega^{-4}, \tag{4}$$

independent of the fetch length, where U_{10} is the wind velocity 10m above sea level and $\alpha_K = 4.5 \times 10^{-3}$. Given that u^* is generally 4 - 7 % of U_{10} in ocean and coastal sites [62], the spectral form determined by Kahma [61] agrees with Toba [59]. Kahma also states that near the peak, the

Electronic copy available at: https://ssrn.com/abstract=4758518

spectra were satisfactorily described by the JONSWAP spectrum, however above frequencies twice the peak frequency the difference becomes significant.

Battjes et al [63] reanalysed the frequency spectra of wind-driven waves observed during JONSWAP to establish whether the ω^{-4} form fits the data better than the ω^{-5} form originally used in the JONSWAP project. The results indicate that the ω^{-4} tail provides a statistically better fit to the observed spectra. In an attempt to clarify the uncertainty between an ω^{-4} or ω^{-5} tail, Liu [64] compared over 2200 spectra obtained from 8 data buoys in the Great Lakes, finding that most values clustered between $\omega^{-3.5}$ and $\omega^{-5.5}$ and concludes that for practical applications ω^{-4} is perhaps an effective approximation. [65] collected spectra from the various wave-growth experiments and reanalysed the data to reconcile the differences in the observed growth rates of wind-generated waves. The analysis showed that the power law of the high frequency tail was not consistent in different datasets, but that the grand average gives a value somewhere between ω^{-4} and ω^{-5}.

Phillips [66] re-examined the nature of the equilibrium range of wave spectra in the wake of the observed discrepencies with his original ω^{-5} formulation. Using recent devevlopments on the dynamical insights into the energy input from the wind, wave-wave interactions and wave breaking, Phillips revised his earlier formulation and concluded that the high frequency spectrum is proportional to $gu^*\omega^{-4}$, in agreeance with the empirical findings of [59] and [61]. The equilibrium range of wave spectra was also theoretically examined by [67], considering a Kolmogorff type of energy cascade from low to high frequencies, also resulting in a wind-dependent frequency spectrum proportional to $gu^*\omega^{-4}$. In the book [68], the various forms proposed for the high frequency tail are reviewed and it is discussed that the parameter values for the PM and JONSWAP spectra are likely chosen artificially high to allow a fit to the ω^{-5} form, rather than ω^{-4}. [68] concludes however, that it is likely there is no universival value n for the ω^{-n} high frequency tail, and that a choice should be made with knowledge of the potential variability.

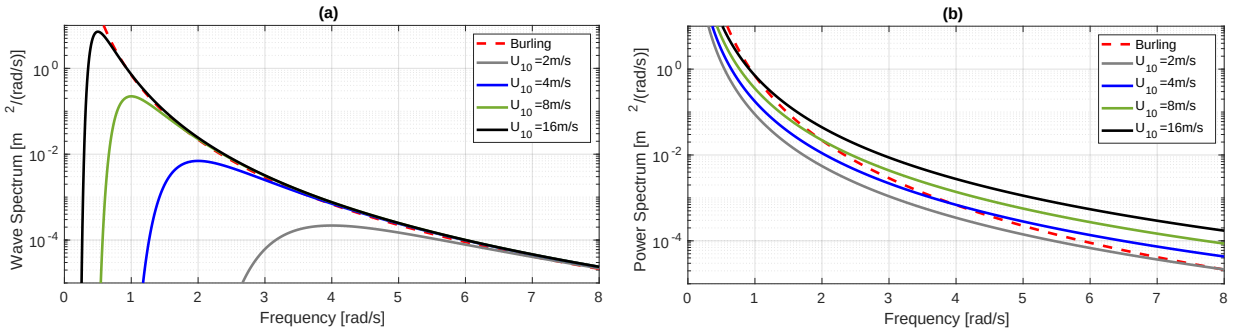


Figure 3. (a) The PM spectrum for varying windspeed compared against Burling's curve, $S_B(\omega)$. (b) Khama's curves, $S_K(\omega)$ for varying wind speed compared against Burling's curve.

Electronic copy available at: https://ssrn.com/abstract=4758518

2.2. The power available in the high frequency tail

The power available in the high frequency tail can be examined via the wave power spectrum, $P_s(\omega)$, which quantifies the power conveyed per meter of wave front for each frequency unit. This spectrum is derived from the standard sea spectrum as follows:

$$P_s(\omega) = \rho g c_g(\omega) S(\omega), \tag{5}$$

where ρ represents the water density, g is the gravitational acceleration, and c_g denotes the wave group velocity. The group velocity is given by:

$$c_g(\omega) = \frac{g}{2\omega}\left(1 + \frac{2kh}{\sinh(kh)}\right)\tanh(kh), \tag{6}$$

with h being the water depth and $k = 2\pi/\omega$ as the wavenumber.

The analysis of the power spectra for both Burling's curve, $S_B(\omega)$, and Kahma's curve, $S_K(\omega)$, across varying wind speeds, is illustrated in Figure 4. For Kahma's curves, there is a noticeable reduction in power per unit frequency, approximately a factor of 8 between 2 and 3 rad/s, followed by a factor of 4 or 5 decrease between 3 and 4 rad/s, and then a further reduction by about a factor of 3 between 4 and 5 rad/s. Burling's curve shows an even more rapid decline in power, diminishing from around 500 W/m per unit frequency at 2 rad/s to about 2 W/m per unit frequency at 5 rad/s.

The power available per meter of wavefront can then be calculated by integrating the wave power spectrum over a given frequency bandwidth, between $\omega_{low} \leq \omega \leq \omega_{high}$:

$$P = \int_{\omega_{low}}^{\omega_{high}} P_s(\omega) d\omega, \tag{7}$$

Figure 5 plots the result of the integral in Eqn 7 for varying bandwidths. Considering Burling's curve, $S_B(\omega_)$, Figure 5 (a) shows that there approximately 200W/m between 2 and 3 rad/s, which then drops by an order of magnitude to around 20W/m between 3 and 4 rad/s and about 5W/m for frequencies above 4 rad/s. Khama's curves for a 2m/s and 8m/s wind speeds, shown in Figure 5 (b) and (c), have power levels lower and higher than Burling's curve, respectively.

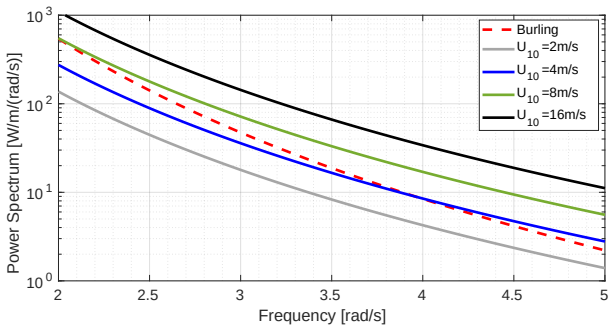


Figure 4. The power spectrum of Khama's curves, $S_K(\omega)$, for varying wind speed, compared against Burling's curve, $S_B(\omega)$.

Electronic copy available at: https://ssrn.com/abstract=4758518

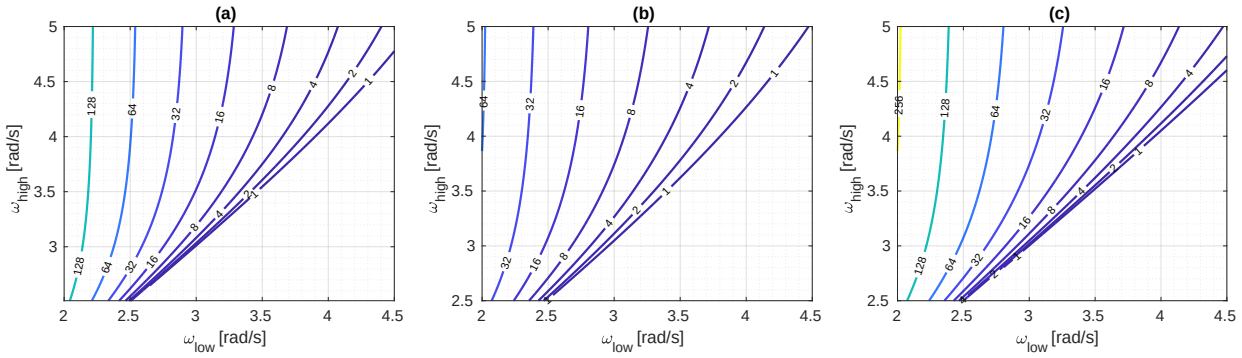


Figure 5. The power [W/m] contained between low and high frequency cut-offs in: (a) Burling's curve, (b) Khama's curve with $U_{10} = 2m/s$ and (c) Khama's curve with $U_{10} = 8m/s$

3. Case study investigation

The theoretical analysis conducted in Section 2 unearthed uncertainties surrounding the high frequency tail of wave spectra, particularly with respect to the diverse formulas proposed to describe this spectral segment. Another critical aspect influencing the utility of wave spectra for MSNs is the precise determination of the high frequency tail's onset, that is, the specific frequency where the tail begins. This cut-off frequency plays a pivotal role, as it directly affects the quantification of power available within the high frequency tail, a factor crucial for its consistent presence both temporally and spatially. Additionally, the phenomenon of energy transfer from lower to higher frequencies as waves approach and interact with shallower coastal waters (see Figure 1(b)), presents another layer of complexity in this context. To shed light on these uncertainties and to gain a deeper understanding of the actual power potential at coastal sites, this section delves into a detailed case study analysis using real-world wave data from multiple coastal locations. This empirical approach is designed to refine our understanding and provide more tangible insights into the feasibility and effectiveness of harvesting wave energy from high frequency spectra in the operational environment of MSNs.

3.1. Case study location

For a comprehensive examination of varying wave resources across potential MSN deployment sites, this study selects the coast of Queensland, Australia, as a focal point. Queensland's extensive coastline, spanning a main length of 6,973 km coupled with an additional 6,374 km of island coastline [69], presents a diverse array of wave conditions. These range from the northern tropical latitudes, which are largely sheltered from the Pacific Ocean by the Great Barrier Reef, to the vigorous southern surf beaches abundant in wave resources, and even include a west-facing coastline in the Gulf of Carpentaria. To capture this diversity, wave data has been sourced from the Queensland Government Department of Science, Information Technology, and Innovation's Coastal Impact Unit, which oversees a network of Waverider buoys positioned at numerous wave monitoring sites across the region [70].

Electronic copy available at: https://ssrn.com/abstract=4758518

The case study specifically examines 12 strategically chosen sites, as indicated in Figure 6. These sites have been selected to cover the entire stretch of Queensland's coastline and to represent a variety of potential MSN deployment scenarios. Factors considered in site selection include sheltered and unsheltered locations, as well as varying water depths, ensuring a comprehensive understanding of the wave resources available across different coastal environments. The details of these sites, including their specific characteristics and geographical locations, are enumerated in Table 1.

Site	Water Depth	Location
(a) Albatross Bay	10m	12° 41.280' S 141° 41.080' E
(b) Skardon River	22m	11° 44.738'S 141° 50.207' E
(c) Cairns	12m	16° 43.830' S 145° 42.910' E
(d) Townsville	17m	19° 09.550' S 147° 03.560' E
(e) Mackay	34m	21° 02.240' S 149° 32.802' E
(f) Mackay Harbour	12m	21° 06.439' S 149° 14.374' E
(g) Gladstone	16m	23° 53.737' S 151° 30.143' E
(h) Bundaberg	18m	24° 40.310' S 152° 30.060' E
(i) Wide Bay	43m	25° 45.620' S 153° 12.198' E
(j) Brisbane	70m	27° 29.230' S 153° 37.900' E
(k) Moreton Bay	10m	27° 14.967' S 153° 11.883' E
(l) Tweed Heads	22m	28° 10.655' S 153° 34.594' E

Table 1. The locations and characteristics of the 12 wave monitoring sites in the case study.

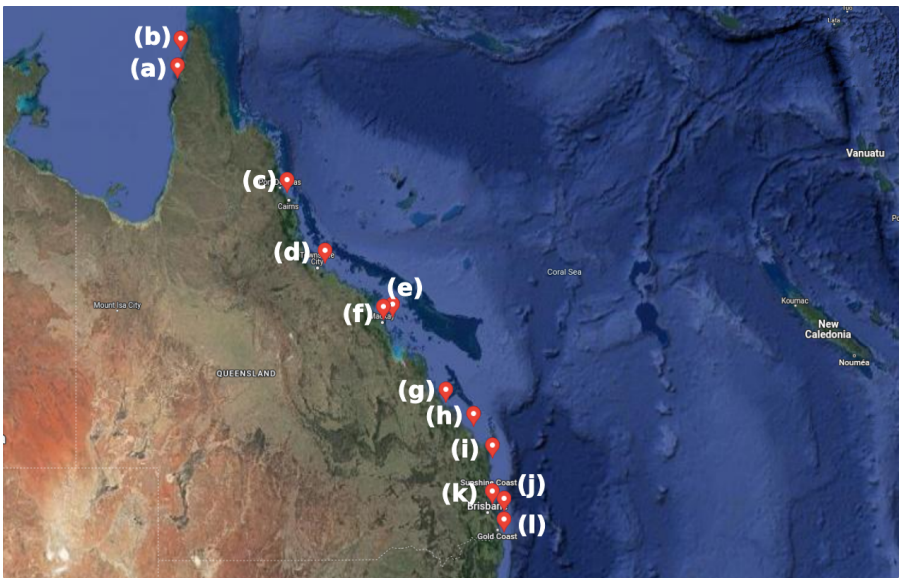


Figure 6. Location of the waverider buoys: (a) Albatross Bay, (b) Skardon River (c) Cairns, (d) Townsville, (e) Mackay, (f) Mackay Harbour, (g) Gladstone, (h) Bundaberg, (i) Wide Bay, (j) Brisbane, (l) Moreton Bay and (l) Tweed Heads. [*Imagery ©2024 TerraMetrics. Map data ©2024 Google*]

Electronic copy available at: https://ssrn.com/abstract=4758518

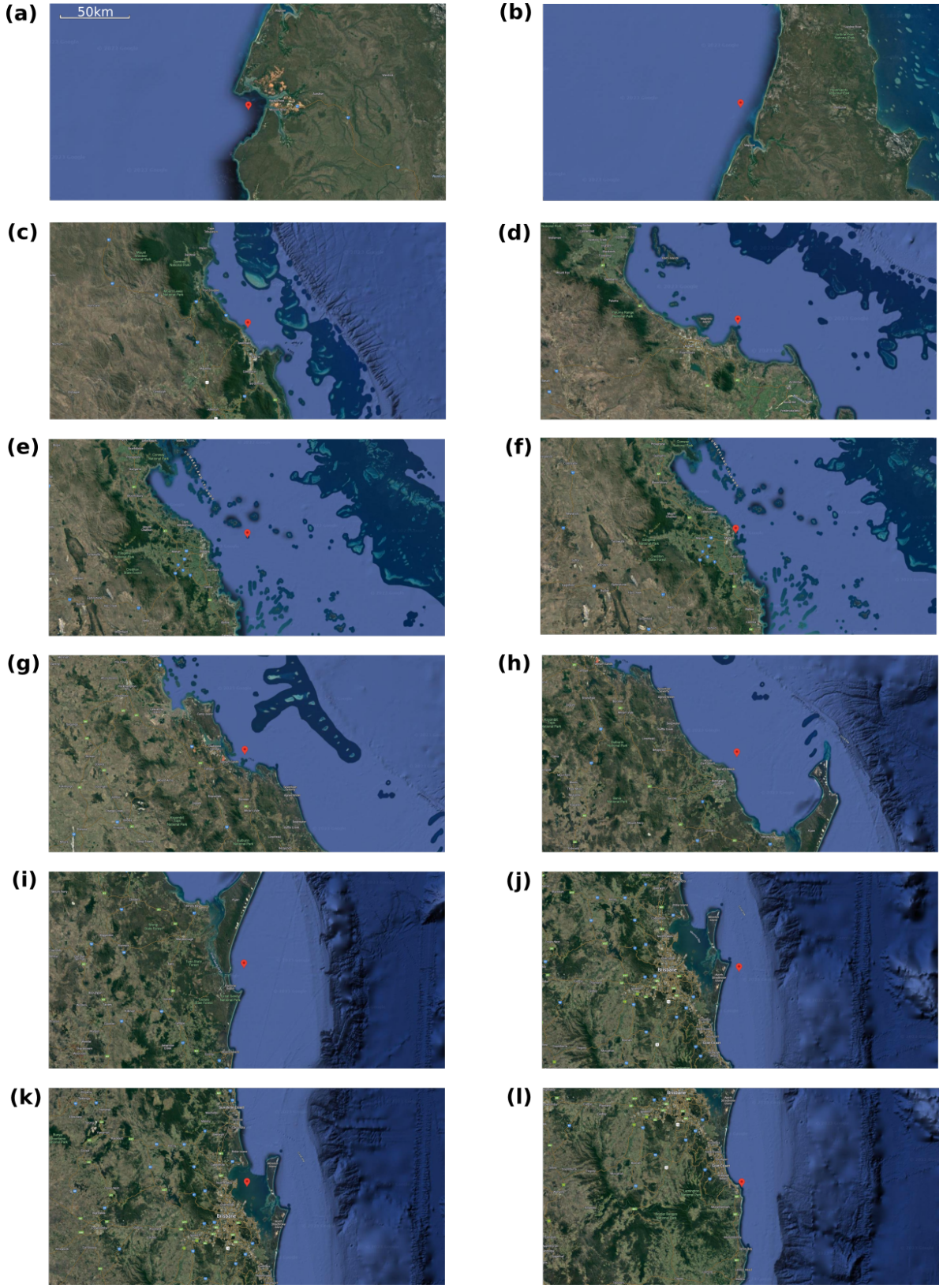


Figure 7. Zoom on the waverider buoy locations: (a) Albatross Bay, (b) Skardon River (c) Cairns, (d) Townsville, (e) Mackay, (f) Mackay Harbour, (g) Gladstone, (h) Bundaberg, (i) Wide Bay, (j) Brisbane, (l) Moreton Bay and (l) Tweed Heads. [*Imagery ©2024 NASA, TerraMetrics. Map data ©2024 Google*]

Electronic copy available at: https://ssrn.com/abstract=4758518

3.2. Wave climates

This subsection delves into the analysis of the sea states recorded at the case study sites, essential for assessing the wave climate at these locations. Sea state data, captured every 30 minutes by Waverider buoys, includes two critical parameters: the peak frequency (ω_p) and the significant wave height (H_s). These are derived from the spectrum calculated from the 30-minute time series of free surface elevation measurements. Over three years of data collection at each site has resulted in a substantial dataset of 17,520 sea state samples per site, which are visualised in the wave scatter diagrams shown in Figure 8. The sea state samples are categorised into bins of 0.2 m for H_s and 0.1 rad/s for ω_p, enabling the calculation of percentage occurrence for each bin to facilitate the production of an occurrence matrix and the corresponding wave scatter diagram.

The analysis serves two primary objectives. The first is to showcase the diversity of sea states across potential MSN deployment sites, highlighting both the range of conditions at individual sites and the variances among different locations. The second, and a principal aim, is to determine the onset frequency of the high frequency tail, which is consistently present across both time and space. To further explore this, Figure 9 illustrates the percentage of time each site experiences peak frequencies exceeding certain values. Combining insights from Figures 8 and 9, along with site descriptions from Section 3.1, reveals that the sites can be categorised into three distinct groups:

- *Sheltered Sites*: Sites (a), (b), and (k) are protected from ocean swells, predominantly featuring peak frequencies above 2 rad/s and significant wave heights below 1m.
- *Partially Sheltered Sites*: Sites (c)-(h) are partially shielded from ocean swells by reefs or islands. Their scatter diagrams show two distinct clusters: one between 1 and 2 rad/s, indicative of local wind seas with decreasing significant wave height at higher frequencies, and a second cluster with lower peak frequencies (0.5 to 1 rad/s) and a small significant wave height, likely representing ocean swells whose wave heights have been attenuated before reaching the site.
- *Open Sites*: Sites (i), (j), and (f) are open to the ocean and predominantly influenced by swells, characterised by low frequencies below 1 rad/s and larger significant wave heights.

Figure 9 further reveals that all sites experience peak frequencies below 3.5 rad/s 95% of the time, and below 3 rad/s at least 90% of the time. Excluding the sheltered sites, the 90% exceedance threshold for peak frequency drops to around 2.2 rad/s. For open sites, the peak frequency is below 1.5 rad/s 99% of the time, underscoring their swell-dominated nature.

Electronic copy available at: https://ssrn.com/abstract=4758518

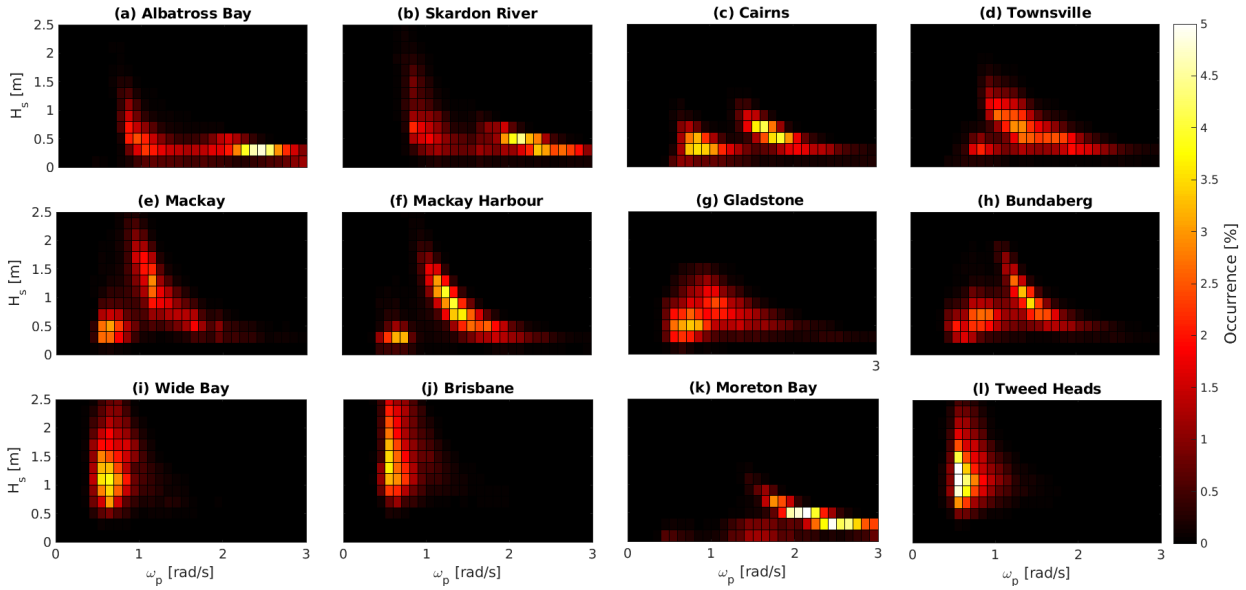


Figure 8. Percentage occurance of sea states parameterised by significant wave height and peak frequency, grouped into 0.1m significant wave height bins and 0.2s peak frequency bins, from 3 years of measurements at the Queensland coast sites.

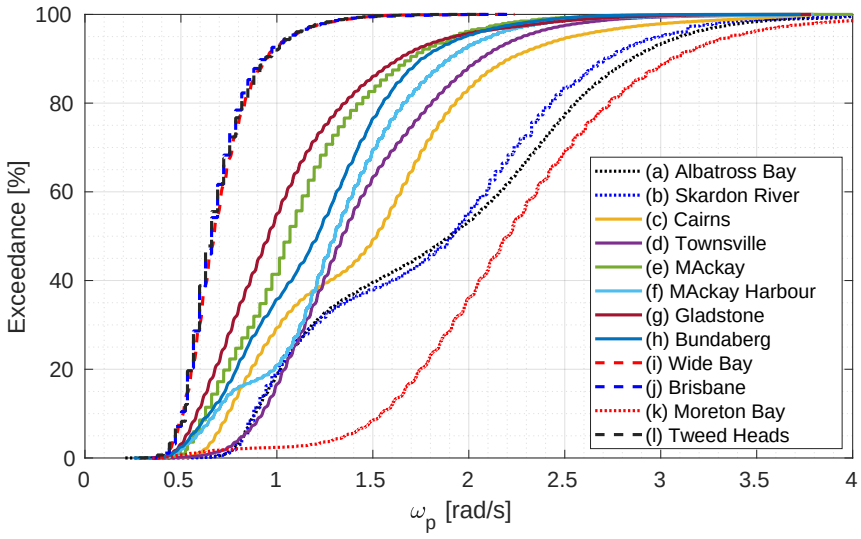


Figure 9. Percentage occurance of sea states parameterised by significant wave height and peak frequency, grouped into 0.1m significant wave height bins and 0.2s peak frequency bins, from 3 years of measurements at the Queensland coast sites.

3.3. Wave Spectra

This subsection moves beyond the derived characterisation parameters for the sea states, H_s and ω_p, to focus on an in-depth analysis of the actual measured wave spectra. By scrutinising the wave spectra, a comprehensive understanding of the distribution of wave energy across different frequency bands at various sites is achieved.

Electronic copy available at: https://ssrn.com/abstract=4758518

3.3.1. Cases

For this analysis, accessing the raw time series data of free surface elevation measurements is essential to generate the spectra. However, unlike the H_s and ω_p data, which is publicly available from the website [70], obtaining the required time series data required personal communications and negotiations due to the sheer volume of files and data involved. Ultimately, one year's worth of free surface elevation measurements, sampled at 0.39 seconds, was procured for each selected site, amounting to over 80 million samples per site. Given the massive data size, the analysis was limited to a select number of sites.

An additional factor influencing site selection was the type of Waverider buoys used: non-directional versus directional. Non-directional buoys, sampling at 0.39 seconds, provide more frequent measurements compared to directional buoys, which sample at 0.78 seconds. This higher sampling rate of non-directional buoys is crucial for investigating the high frequency tail of the wave spectrum. Consequently, only sites equipped with non-directional buoys were chosen for this detailed spectral analysis. Out of these, data from five sites were obtained, ensuring a representative sample across different coastal environments. These sites include Moreton Bay from the sheltered category, Cairns and Mackay representing partially sheltered sites, and Brisbane and Tweed Heads as examples of open sites.

3.3.2. Analysis

The analysis considers the wave power spectra, $P_s(\omega)$, which is derived for 30 minute intervals, using the free surface elevation sampled at 0.39 seconds. Example spectra for the five sites are displayed in the contour plots in the left and middle columns of Figure 10. The contour plots have time on the vertical axis, showing the evolution of the wave spectra over one week. The left column depicts a week during the summer months and the middle column one from the winter months. The plots highlight the variability of the spectra over time and betwen locations.

A complementary contour plot in the right column of Figure 10 offers a broader, year-long perspective. It shows the percentage of time that the power spectrum at various frequencies exceeded different orders of magnitude over the course of an entire year. This plot reveals significant disparities in available power at lower frequencies among the sites. However, at higher frequencies, particularly above 2.5 rad/s, a notable consistency emerges in both the magnitude of the power spectra and its percentage occurrence across different sites. This observation substantiates the central thesis of this study, emphasising the more uniform nature of the high frequency tail of wave spectra. This consistency, despite the diversity of the sites, underscores the potential of high frequency waves as a reliable source of energy for MSNs.

Electronic copy available at: https://ssrn.com/abstract=4758518

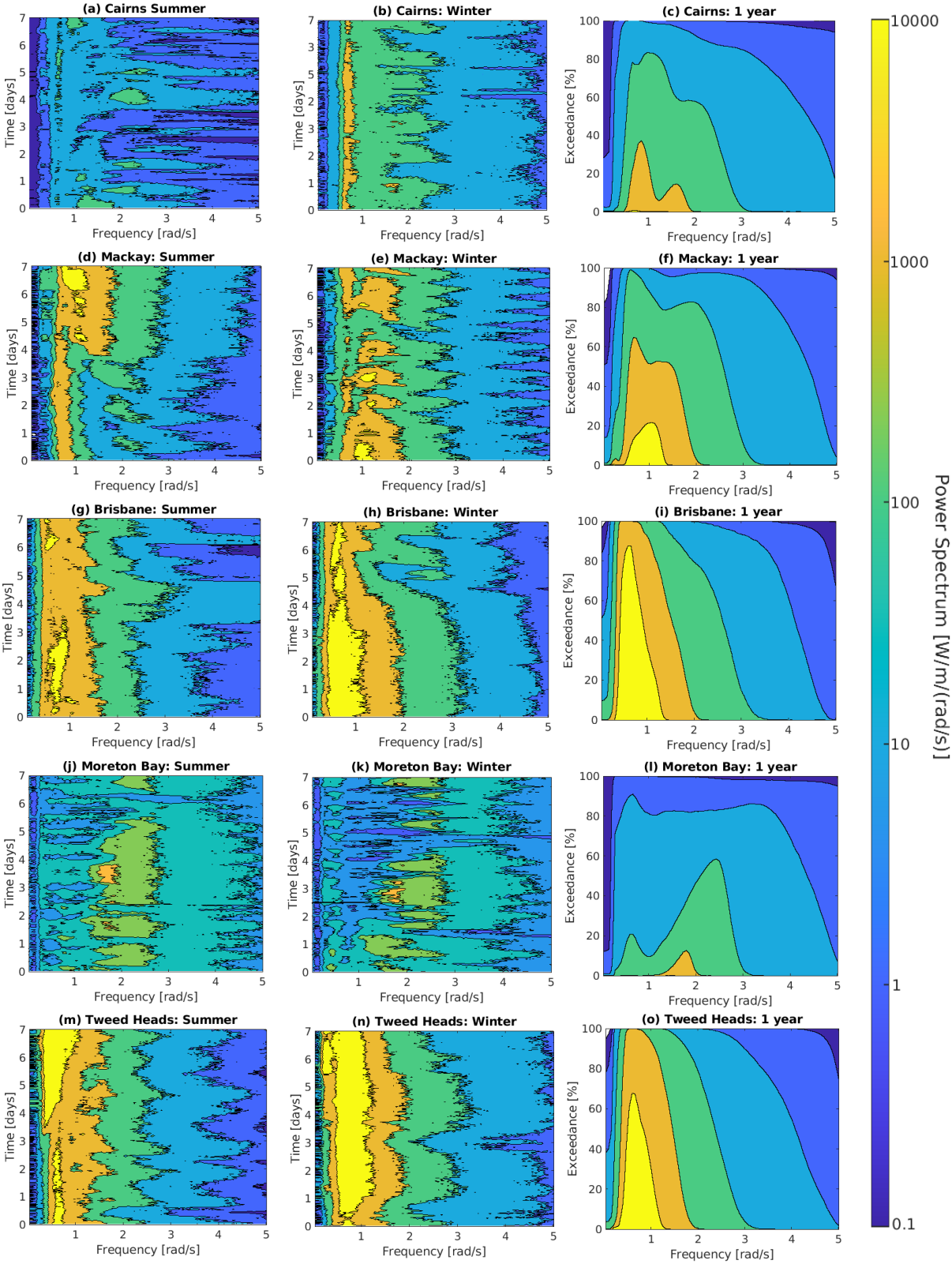


Figure 10. An example of the power spectrum and its evolution over one week, during summer (left column) and winter (middle column), at five different locations (rows). The percentage of time, over one year, that the power exceeded certain levels at a given frequency is then plotted in the right column.

Electronic copy available at: https://ssrn.com/abstract=4758518

The spatial consistency of the high frequency tail is further highlighted in Figure 11, where the mean value of the power spectra, averaged over a year, is plotted for the five sites. A key observation from this figure is the convergence of the power spectra to similar values at frequencies above 2 rad/s, despite significant variations at lower frequencies among the different sites. This demonstrates the spatial uniformity of the high frequency tail across diverse coastal locations, reinforcing its potential as a consistent energy resource for MSNs.

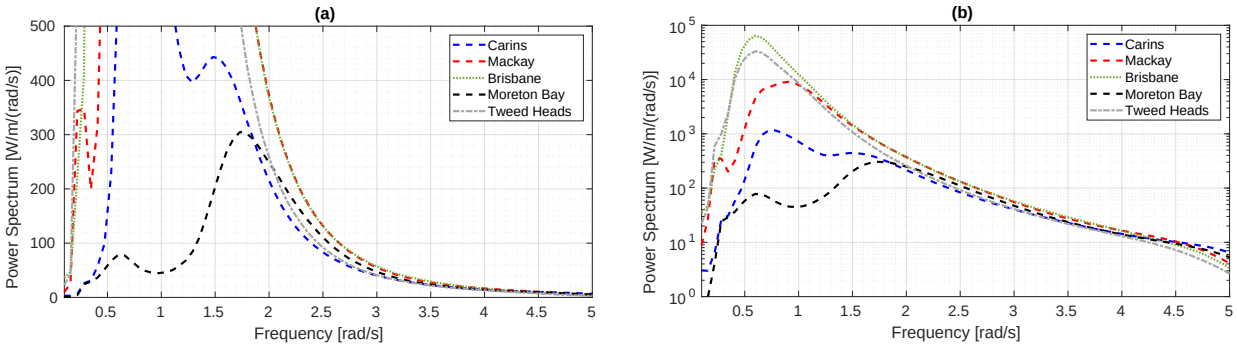


Figure 11. The mean power spectrum for the five sites (a) Linear scale (b) Log scale.

Further emphasising the reliability of the high frequency tail, the temporal consistency of the power spectra is examined in Figure 12, which plots the coefficient of variability (COV) of the power spectra for each site. The COV measures the variation of the power spectra value at each frequency over the years worth of data and is defined as the percentage ratio of the standard deviation (STD) and the mean:

$$COV(\omega) = \frac{STD(\omega)}{mean(\omega)} \times 100 \tag{8}$$

The COV plots in Figure 12 reveal high variability in the power spectra at lower frequencies for each site. However, a noteworthy consistency is observed at frequencies above 2.5 rad/s, where the COV reaches a minimum. This finding highlights the temporal stability of the power spectra in this high frequency range throughout the year. The subsequent increase in COV at frequencies above 4 rad/s for sites experiencing large swell waves (Tweed Heads, Brisbane, and Mackay), is likely an artifact of the Waverider buoy and is discussed further in Section 4).

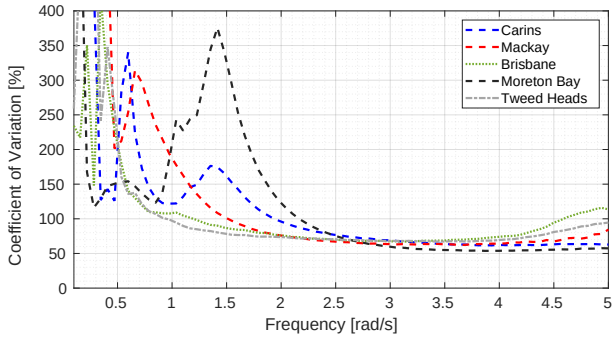


Figure 12. The coefficient of variation, over 1 year, for the five selected locations.

Electronic copy available at: https://ssrn.com/abstract=4758518

Finally, the most important aspect for wave energy harvesting for MSNs is the power availability, which is examined in Figure 13. Here the exceedance probability is plotted for the wave power per meter contained between different frequency bands. In the frequency band of 2.5 to 3.5 rad/s, as shown in Figure 13 (a), the power exceeds 40-60W/m for 50% of the time, 15-30W/m for 80% of the time, and 6-18W/m for 90% of the time across all sites. This data suggests a relatively high power output in this frequency range, albeit with some variation across different locations. Moving to a higher frequency band of 3 to 4 rad/s in Figure 13 (b), the power exceeds 21-27W/m for 50% of the time, 10-15W/m for 80% of the time, and 5-10W/m for 90% of the time across all sites. This band shows a trend towards more uniform power availability across different sites, indicating a potential consistency in wave energy resources. In the higher frequency band of 3.5 to 4.5 rad/s, depicted in Figure 13 (c), the power exceeds 12-15W/m for 50% of the time, 6-8W/m for 80% of the time, and 3-6W/m for 90% of the time across the sites. This trend of decreasing variability in power between sites as the frequency increases is notable. It suggests that higher frequency bands, while providing lower overall power output, offer a more consistent and predictable wave energy resource.

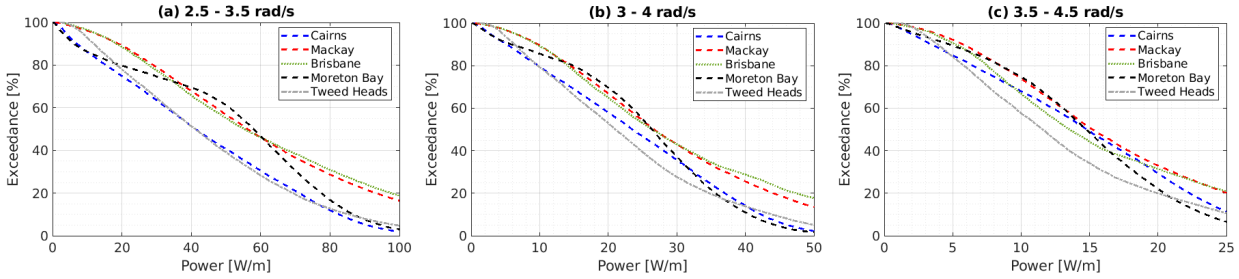


Figure 13. Comparison of the time percentance the power spectra in the high frequency tail exceeded 1W, 10W and 100W, for the five selected locations.

For a more detailed inspection of the power availability, with more flexibility in the choice of frequency bands, Figure 14 presents exceedance probability contours. These contours vary according to the low frequency cut-off, ω_{low}, and the high frequency cut-off, ω_{high}, across different power levels: 5W/m (left column), 10W/m (middle column), and 20W/m (right column). The data is organised for the five distinct sites (rows). As discussed in Section 1.3and illustrated in Figure 2, small scale WECs often have high resonant frequencies and narrow bandwidths. Figure 14 thus offers an opportunity to assess the available power across various bandwidths and resonant frequencies.

For instance, if a WEC is designed to be broadband, capturing power between 2.5 and 5 rad/s, then more than 5W/m is available over 95% of the time at all sites, over 10W/m more than 90% of the time, and over 20W/m more than 80% of the time. Conversely, for a more narrowband WEC operating at higher frequencies, such as between 3.5 and 4 rad/s, the power availability is reduced: over 5W/m is achievable only about 70% of the time, over 10W/m less than 50% of the time, and over 20W/m less than 10% of the time.

Electronic copy available at: https://ssrn.com/abstract=4758518

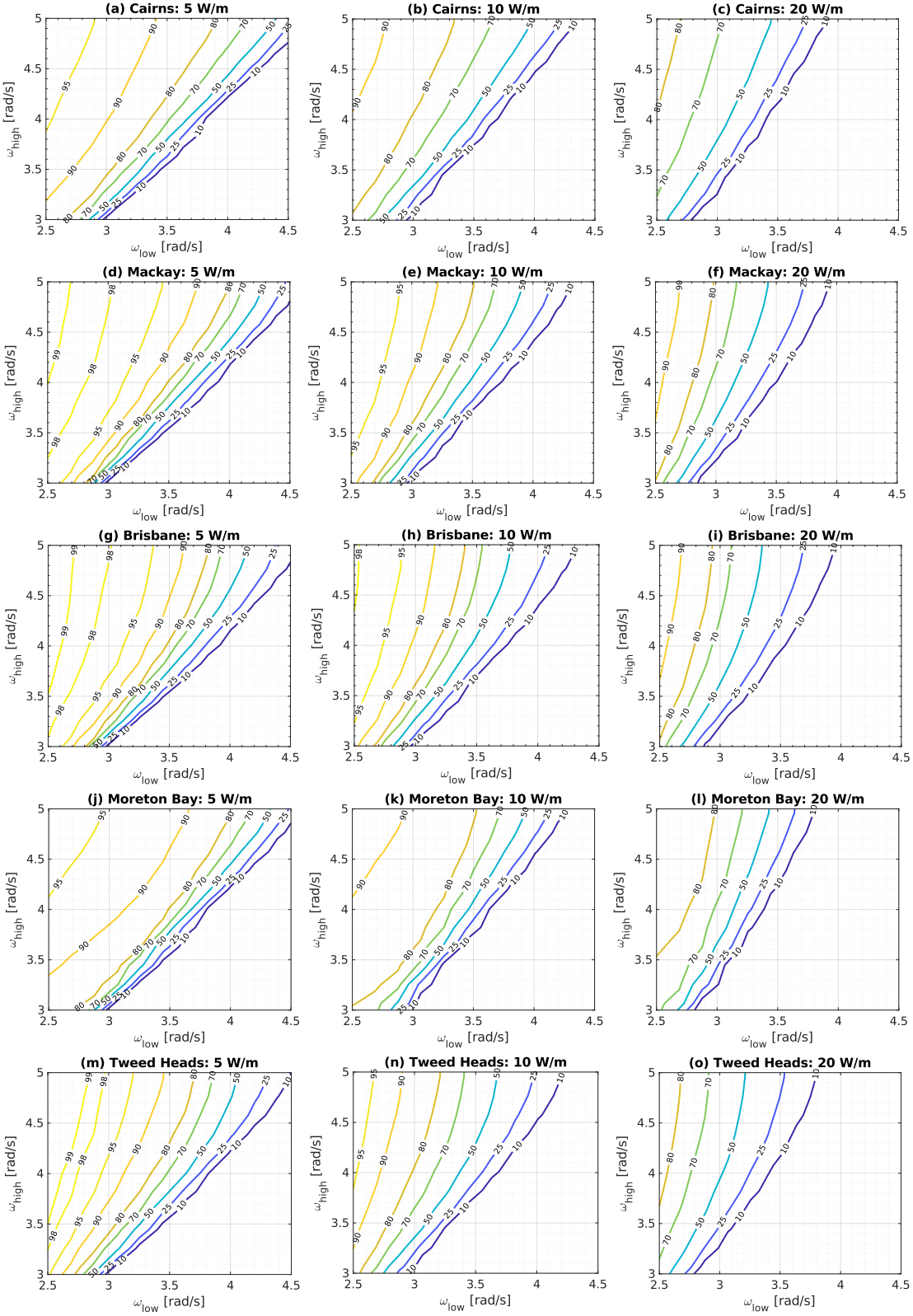


Figure 14. Contours of the time percentage the power spectra exceeded 5W/m (left columm), 10W/m (middle column) and 20W/m (right column), as a function of the high and low frequency cut-offs, for the five selected locations (rows).

Electronic copy available at: https://ssrn.com/abstract=4758518

4. Discussion

This investigation aimed to identify a consistently present frequency band in the tail of sea spectra for effective wave energy harvesting. The focus was on small-scale wave energy harvesters, designed to operate efficiently within this bandwidth, thereby ensuring a robust and consistent power output across various deployment conditions. Our study sought to quantify the available power in this frequency range to inform the potential outputs of such a wave energy harvester.

The literature review, in Section 2.1, revealed some discrepancies regarding the high frequency tail of wave spectra, with a consensus forming around a spectral form between ω^{-4} to ω^{-5}. However, the defining factor for available power and resource characteristics is the start frequency of this high frequency tail, which our data analysis of 12 diverse coastal sites over three years showed that peak frequencies rarely exceed 3 rad/s. The exceedance curves (Figure 9) typically had a knee less than 2.5 rad/s, with only very sheltered sites slightly higher, around 3 rad/s. The investigation into actual wave power spectra, based on a year's data from five locations, underscored the convergence of mean power spectra around 2.5 rad/s. This convergence demonstrates spatial uniformity between different sites and temporal consistency, with low standard deviation across each site's yearly data for frequencies above this 2.5 rad/s threshold.

Quantifying the available power in the high-frequency tail, we found over 20W/m available above 2.5 rad/s for more than 85% of the time across all sites, exceeding 10W/m 92% of the time and over 5W/m more than 96% of the time. The absorbed power by a wave energy harvester depends on:

- *The capture width*: the extent over which it absorbs power from the wavefront. The theoretical maximum capture width for a point absorber, is the wavelength divided by 2π [71, 72], which varies from approximately 1.5m at 2.5 rad/s to 0.4m at 5 rad/s.

- *The bandwidth*: the frequency range over which the WEC effectively absorbs wave power. Optimal performance occurs at the resonant frequency, with diminishing efficacy as the frequency deviates from this point. The inclusion of control techniques [73] can broaden the bandwidth but introduce a trade-off relating to the simplicity of the device.

The plots in Figure 14 are intended to offer some guidance on the effect of resonant frequency and bandwidth on the available power.

A potential benefit for nearshore sites was proposed in Section 1.3, relating to a second spectral peak at twice the frequency of the main wave (see Figure 1(b)), which might enhance the energy resource in the high frequency band of wave spectra for powering MSNs. However, our subsequent investigation found that the consistent high-frequency tail in wave spectra predominantly exists above 2.5 rad/s. In contrast, the peak frequencies of coastal swell waves are typically well below 1 rad/s. This disparity indicates that the anticipated benefit from secondary spectral peaks in

Electronic copy available at: https://ssrn.com/abstract=4758518

nearshore regions may not materialise, as these peaks fall outside the higher frequency range identified as consistently present and useful for energy harvesting in MSNs.

An important aspect warranting further discussion is the capability of standard Waverider buoys to accurately measure high-frequency tails. While mean values in Figure 11 show convergence starting around 2.5 rad/s, at higher frequencies, above 4 rad/s, sites with larger swell waves diverge from this trend. This observation, along with the increasing coefficient of variability for these sites (Figure 12), is attributed to the Waverider buoys' reduced capability to capture higher spectral harmonics, as detailed in Tucker and Pitt [74] and further explained in [75].

Looking forward, based on the findings from this study, designing wave energy harvesters that leverage the high-frequency tail of ocean wave spectra presents a promising avenue for creating robust solutions to power MSNs. Optimising the design of a wave energy harvester to this frequency band is the scope of future work, however, preliminary research suggests targeting waves above 3 rad/s could consistently deliver over 1W of power from a 40 kg wave power buoy with 50% electrical power-take off (PTO) efficiency [25]. This opens new possibilities for designing efficient and sustainable MSNs, particularly in regions where traditional renewable energy sources may be less effective. The insights gained from this investigation lay a foundation for further advancements in the field of wave energy harvesting, potentially leading to more robust and adaptable coastal monitoring systems.

5. Conclusion

This study offers a pragmatic assessment of the viability of wave energy harvesters for use in MSNs. Our investigation underscores that, unlike large-scale WECs which are tuned to the dominant wave frequencies, the design and operational limitations of small-scale wave energy harvesters render them more suitable for higher frequencies. Importantly, we have identified the high-frequency tail of ocean wave spectra as a largely consistent resource across different marine environments, aligning well with the operational range of these small-scale wave energy harvesters.

This research has demonstrated that there is a significant and persistent amount of power available in the high-frequency region of ocean wave spectra, which can be efficiently harnessed by appropriately designed small-scale wave energy harvesters. The quantification of power in the high-frequency tail, particularly above 2.5 rad/s, shows potential for consistent power availability across a wide range of coastal sites. This aligns with the need for MSNs to have a reliable and sustainable renewable energy source, independent of the variability inherent in coastal wave climates. By harnessing the omnipresent nature of the high-frequency tail of ocean wave spectra, there is an opportunity to develop wave energy harvesters that provide a robust, universally applicable, and sustainable solution for powering MSNs.

Electronic copy available at: https://ssrn.com/abstract=4758518

Acknowledgements

Vincenzo Nava is funded by the Spanish Ministry of Economic Affairs and Digital Transformation in the framework of IA4TES project (with reference number MIA.2021.M04.008, as well as the Spanish Ministry of Science and Innovation projects with references TED2021-132783B-I00 and PID2019-108111RB-I00 (FEDER/AEI). The study has also carried out within the "BCAM Severo Ochoa" accreditation of excellence CEX2021-001142-S / MICIN / AEI / 10.13039/501100011033; and the Basque Government through the BERC 2022-2025 program.

Josh Davidson is funded by MCIN and by the European Union NextGenerationEU/PRTR-C17.I1, as well as by IKUR Strategy under the collaboration agreement between Ikerbasque Foundation and BCAM on behalf of the Department of Education of the Basque Government. Josh Davidson would also like to express his gratitude to Peter Ridd for the mentorship and supervision which were key factors in the formation of this study.

Data availability

Data may be made available upon request.

References

[1] T. B. Curtin, J. G. Bellingham, J. Catipovic, D. Webb, Autonomous oceanographic sampling networks, Oceanography 6 (3) (1993) 86–94.

[2] S. Rajasegarar, J. Gubbi, O. Bondarenko, S. Kininmonth, S. Marusic, S. Bainbridge, I. Atkinson, M. Palaniswami, Sensor network implementation challenges in the great barrier reef marine environment, in: Proceedings of the ICT-MobileSummit 2008 Conference, 2008.

[3] R. Johnstone, D. Caputo, U. Cella, A. Gandelli, C. Alippi, F. Grimaccia, N. Haritos, R. E. Zich, et al., Smart environmental measurement & analysis technologies (semat): Wireless sensor networks in the marine environment, Proceedings of the Wireless Sensor and Actuator Network Research on Opposite Sides of the Globe (SENSEI) (2008).

[4] U. M. Cella, N. Shuley, R. Johnstone, Wireless sensor networks in coastal marine environments: a study case outcome, in: Proceedings of the Fourth ACM International Workshop on UnderWater Networks, 2009.

[5] T. Myers, I. Atkinson, R. Johnstone, Semantically enabling the semat project: extending marine sensor networks for decision support and hypothesis testing, in: Complex, Intelligent and Software Intensive Systems (CISIS), 2010 International Conference on, IEEE, 2010, pp. 974–979.

[6] J. Trevathan, R. Johnstone, T. Chiffings, I. Atkinson, N. Bergmann, W. Read, S. Theiss, T. Myers, T. Stevens, Semat â€" the next generation of inexpensive marine environmental monitoring and measurement systems, Sensors 12 (7) (2012) 9711–9748. doi:10.3390/s120709711.
URL http://www.mdpi.com/1424-8220/12/7/9711

[7] K. Liu, Z. Yang, M. Li, Z. Guo, Y. Guo, F. Hong, X. Yang, Y. He, Y. Feng, Y. Liu, Oceansense: Monitoring the sea with wireless sensor networks, ACM SIGMOBILE Mobile Computing and Communications Review 14 (2) (2010) 7–9.

[8] Z. Yang, M. Li, Y. Liu, Sea depth measurement with restricted floating sensors, in: 28th IEEE International Real-Time Systems Symposium (RTSS 2007), IEEE, 2007, pp. 469–478.

Electronic copy available at: https://ssrn.com/abstract=4758518

[9] O. Bondarenko, S. Kininmonth, M. Kingsford, Underwater sensor networks, oceanography and plankton assemblages, in: Intelligent Sensors, Sensor Networks and Information, 2007. ISSNIP 2007. 3rd International Conference on, IEEE, 2007, pp. 657–662.

[10] H. Chi, Y. Du, P. M. Brett, Design of a marine environment monitoring system based on the internet of things, Journal of Coastal Research 110 (SI) (2020) 256–260.

[11] H. Luo, K. Wu, Z. Guo, L. Gu, L. M. Ni, Ship detection with wireless sensor networks, IEEE Transactions on Parallel and Distributed Systems 23 (7) (2011) 1336–1343.

[12] M. Marin-Perianu, S. Chatterjea, R. Marin-Perianu, S. Bosch, S. Dulman, S. Kininmonth, P. Havinga, Wave monitoring with wireless sensor networks, in: 2008 International Conference on Intelligent Sensors, Sensor Networks and Information Processing, IEEE, 2008, pp. 611–616.

[13] E. S. Haq, D. Suwardiyanto, M. D. Ayatullah, E. M. Rini, H. Sutiksno, E. Setyati, The coastal early warning system based on buoy sensor measurement, in: 2019 2nd International Conference of Computer and Informatics Engineering (IC2IE), IEEE, 2019, pp. 39–43.

[14] P. Barbosa, N. White, N. Harris, Wireless sensor network for localized maritime monitoring, in: Advanced Information Networking and Applications - Workshops, 2008. AINAW 2008. 22nd International Conference on, 2008.

[15] J. Lloret, S. Sendra, M. Garcia, G. Lloret, Group-based underwater wireless sensor network for marine fish farms, in: GLOBECOM Workshops (GC Wkshps), 2011 IEEE, IEEE, 2011, pp. 115–119.

[16] H. Yang, H. Wu, Y. He, Architecture of wireless sensor network for monitoring aquatic environment of marine shellfish, in: 2009 7th Asian Control Conference, IEEE, 2009, pp. 1147–1151.

[17] J. Tateson, C. Roadknight, A. Gonzalez, T. Khan, S. Fitz, I. Henning, N. Boyd, C. Vincent, I. Marshall, Real world issues in deploying a wireless sensor network for oceanography, REALWSN 2005 (2005).

[18] C. A. Pérez, F. S. Valles, R. T. Sánchez, M. J. Buendía, F. López-Castejón, J. G. Cervera, Design and deployment of a wireless sensor network for the mar menor coastal observation system, IEEE Journal of Oceanic Engineering 42 (4) (2017) 966–976.

[19] C. Albaladejo, P. SÃ¡nchez, A. Iborra, F. Soto, J. A. LÃ³pez, R. Torres, Wireless sensor networks for oceanographic monitoring: A systematic review, Sensors 10 (7) (2010) 6948–6968. doi:10.3390/s100706948.
URL http://www.mdpi.com/1424-8220/10/7/6948

[20] G. Xu, W. Shen, X. Wang, Applications of wireless sensor networks in marine environment monitoring: A survey, Sensors 14 (9) (2014) 16932–16954.

[21] J. P. Mishra, K. Singh, H. Chaudhary, Research advancements in ocean environmental monitoring systems using wireless sensor networks: a review, TELKOMNIKA (Telecommunication Computing Electronics and Control) 21 (3) (2023) 513–527.

[22] P. Gupta, J. Batra, J. Sangwan, A. Khatri, Marine monitoring based on wsn: application and challenges, International Journal of Advanced Studies of Scientific Research 3 (12) (2018).

[23] C. Knight, J. Davidson, S. Behrens, Energy options for wireless sensor nodes, Sensors 8 (2008) 8037–8066.

[24] F. K. Shaikh, S. Zeadally, Energy harvesting in wireless sensor networks: A comprehensive review, Renewable and Sustainable Energy Reviews 55 (2016) 1041–1054.

[25] J. Davidson, Energy harvesting for marine based sensors, Ph.D. thesis, James Cook University (2016).

[26] R. Pelc, R. M. Fujita, Renewable energy from the ocean, Marine Policy 26 (6) (2002) 471–479.

[27] T. Voigt, F. Österlind, N. Finne, N. Tsiftes, Z. He, J. Eriksson, A. Dunkels, U. Båmstedt, J. Schiller, K. Hjort, Sensor networking in aquatic environments-experiences and new challenges, in: Local Computer Networks, 2007. LCN 2007. 32nd IEEE Conference on, IEEE, 2007, pp. 793–798.

[28] R. Xu, H. Wang, Z. Xi, W. Wang, M. Xu, Recent progress on wave energy marine buoys, Journal of Marine Science and Engineering 10 (5) (2022) 566.

[29] L. A. Gish, Concept design of a small heaving oscillating water column wave energy converter, in: Global Oceans

Electronic copy available at: https://ssrn.com/abstract=4758518

2020: Singapore–US Gulf Coast, IEEE, 2020, pp. 1–5.

[30] L. Wang, J. Lin, H. Li, J. Jiang, S. Wu, G. Lu, Achieving efficient power generation for an enclosed drifting buoy by multi-dof wave energy harvesting, Available at SSRN 4325652.

[31] C. Albaladejo, F. Soto, R. Torres, P. SÃ¡nchez, J. A. LÃ³pez, A low-cost sensor buoy system for monitoring shallow marine environments, Sensors 12 (7) (2012) 9613–9634. doi:10.3390/s120709613.
URL http://www.mdpi.com/1424-8220/12/7/9613

[32] T. Zhao, M. Xu, X. Xiao, Y. Ma, Z. Li, Z. L. Wang, Recent progress in blue energy harvesting for powering distributed sensors in ocean, Nano Energy 88 (2021) 106199.

[33] I. McLeod, J. V. Ringwood, Powering data buoys using wave energy: a review of possibilities, Journal of Ocean Engineering and Marine Energy 8 (3) (2022) 417–432.

[34] O. M. Phillips, The equilibrium range in the spectrum of wind-generated waves, Journal of Fluid Mechanics 4 (1958) 426–434.

[35] K. Hasselmann, T. Barnett, E. Bouws, H. Carlson, D. Cartwright, K. Enke, J. Ewing, H. Gienapp, D. Hasselmann, P. Kruseman, et al., Measurements of wind-wave growth and swell decay during the joint north sea wave project (jonswap), Tech. rep. (1973).

[36] M. Folley, T. Whittaker, Analysis of the nearshore wave energy resource, Renewable Energy 34 (7) (2009) 1709–1715.

[37] K. Kevin, E. F. Simanjuntak, A. R. Utomo, F. Husnayain, F. H. Jufri, D. R. Aryani, Study on micro-scale ocean wave power generator using oscillating water column system with piezoelectric, in: 2020 8th International Electrical Engineering Congress (iEECON), IEEE, 2020, pp. 1–4.

[38] Y. Masuda, An experience of wave power generator through tests and improvement, in: D. V. Evans, A. F. O. de Falcão (Eds.), Hydrodynamics of Ocean Wave-Energy Utilization, Springer Berlin Heidelberg, Berlin, Heidelberg, 1986, pp. 445–452.

[39] F. Zeng, T. Wang, In-situ wave energy harvesting for unmanned marine devices: A review, Ocean Engineering 285 (2023) 115376.

[40] C. Rodrigues, D. Nunes, D. Clemente, N. Mathias, J. Correia, P. Rosa-Santos, F. Taveira-Pinto, T. Morais, A. Pereira, J. Ventura, Emerging triboelectric nanogenerators for ocean wave energy harvesting: state of the art and future perspectives, Energy & Environmental Science 13 (9) (2020) 2657–2683.

[41] H. Wang, Z. Fan, T. Zhao, J. Dong, S. Wang, Y. Wang, X. Xiao, C. Liu, X. Pan, Y. Zhao, et al., Sandwich-like triboelectric nanogenerators integrated self-powered buoy for navigation safety, Nano Energy 84 (2021) 105920.

[42] H. Shao, Z. Wen, P. Cheng, N. Sun, Q. Shen, C. Zhou, M. Peng, Y. Yang, X. Xie, X. Sun, Multifunctional power unit by hybridizing contact-separate triboelectric nanogenerator, electromagnetic generator and solar cell for harvesting blue energy, Nano Energy 39 (2017) 608–615.

[43] X. Liang, T. Jiang, G. Liu, Y. Feng, C. Zhang, Z. L. Wang, Spherical triboelectric nanogenerator integrated with power management module for harvesting multidirectional water wave energy, Energy & Environmental Science 13 (1) (2020) 277–285.

[44] W. Liu, L. Xu, T. Bu, H. Yang, G. Liu, W. Li, Y. Pang, C. Hu, C. Zhang, T. Cheng, Torus structured triboelectric nanogenerator array for water wave energy harvesting, Nano Energy 58 (2019) 499–507.

[45] M. Xu, T. Zhao, C. Wang, S. L. Zhang, Z. Li, X. Pan, Z. L. Wang, High power density tower-like triboelectric nanogenerator for harvesting arbitrary directional water wave energy, ACS nano 13 (2) (2019) 1932–1939.

[46] J. An, Z. M. Wang, T. Jiang, X. Liang, Z. L. Wang, Whirling-folded triboelectric nanogenerator with high average power for water wave energy harvesting, Advanced Functional Materials 29 (39) (2019) 1904867.

[47] X. Liang, T. Jiang, G. Liu, T. Xiao, L. Xu, W. Li, F. Xi, C. Zhang, Z. L. Wang, Triboelectric nanogenerator networks integrated with power management module for water wave energy harvesting, Advanced Functional Materials 29 (41) (2019) 1807241.

[48] X. Chen, L. Gao, J. Chen, S. Lu, H. Zhou, T. Wang, A. Wang, Z. Zhang, S. Guo, X. Mu, et al., A chaotic

Electronic copy available at: https://ssrn.com/abstract=4758518

pendulum triboelectric-electromagnetic hybridized nanogenerator for wave energy scavenging and self-powered wireless sensing system, Nano Energy 69 (2020) 104440.

[49] P. Cheng, H. Guo, Z. Wen, C. Zhang, X. Yin, X. Li, D. Liu, W. Song, X. Sun, J. Wang, et al., Largely enhanced triboelectric nanogenerator for efficient harvesting of water wave energy by soft contacted structure, Nano Energy 57 (2019) 432–439.

[50] F. Xi, Y. Pang, G. Liu, S. Wang, W. Li, C. Zhang, Z. L. Wang, Self-powered intelligent buoy system by water wave energy for sustainable and autonomous wireless sensing and data transmission, Nano Energy 61 (2019) 1–9.

[51] Z. Lin, B. Zhang, H. Guo, Z. Wu, H. Zou, J. Yang, Z. L. Wang, Super-robust and frequency-multiplied triboelectric nanogenerator for efficient harvesting water and wind energy, Nano Energy 64 (2019) 103908.

[52] G. Liu, H. Guo, S. Xu, C. Hu, Z. L. Wang, Oblate spheroidal triboelectric nanogenerator for all-weather blue energy harvesting, Advanced Energy Materials 9 (26) (2019) 1900801.

[53] L. Feng, G. Liu, H. Guo, Q. Tang, X. Pu, J. Chen, X. Wang, Y. Xi, C. Hu, Hybridized nanogenerator based on honeycomb-like three electrodes for efficient ocean wave energy harvesting, Nano Energy 47 (2018) 217–223.

[54] Z. Saadatnia, E. Asadi, H. Askari, E. Esmailzadeh, H. E. Naguib, A heaving point absorber-based triboelectric-electromagnetic wave energy harvester: An efficient approach toward blue energy, International Journal of Energy Research 42 (7) (2018) 2431–2447.

[55] C. Hou, T. Chen, Y. Li, M. Huang, Q. Shi, H. Liu, L. Sun, C. Lee, A rotational pendulum based electromagnetic/triboelectric hybrid-generator for ultra-low-frequency vibrations aiming at human motion and blue energy applications, Nano Energy 63 (2019) 103871.

[56] H. Wang, Q. Zhu, Z. Ding, Z. Li, H. Zheng, J. Fu, C. Diao, X. Zhang, J. Tian, Y. Zi, A fully-packaged ship-shaped hybrid nanogenerator for blue energy harvesting toward seawater self-desalination and self-powered positioning, Nano Energy 57 (2019) 616–624.

[57] R. W. Burling, Wind generation of waves on water, Ph.D. thesis, Imperial College, University of London (1955).

[58] W. J. Pierson Jr, L. Moskowitz, A proposed spectral form for fully developed wind seas based on the similarity theory of sa kitaigorodskii, Tech. rep. (1963).

[59] Y. Toba, Local balance in the air-sea boundary processes - iii on the spectrum of wind waves, Journal of the Oceanographical Society of Japan 29 (5) (1973) 209–220.

[60] S. Kawai, K. Okada, Y. Toba, Field data support of three-seconds power law andgu* σ- 4-spectral form for growing wind waves, Journal of the Oceanographical Society of Japan 33 (3) (1977) 137–150.

[61] K. K. Kahma, A study of the growth of the wave spectrum with fetch, Journal of Physical Oceanography 11 (11) (1981) 1503–1515.

[62] R. J. Foreman, S. Emeis, Revisiting the definition of the drag coefficient in the marine atmospheric boundary layer, Journal of Physical Oceanography 40 (10) (2010) 2325–2332.

[63] J. Battjes, T. Zitman, L. Holthuusen, A reanalysis of the spectra observed in jonswap, Journal of physical oceanography 17 (8) (1987) 1288–1295.

[64] P. C. Liu, On the slope of the equilibrium range in the frequency spectrum of wind waves, Journal of Geophysical Research: Oceans 94 (C4) (1989) 5017–5023.

[65] K. K. Kahma, C. J. Calkoen, Reconciling discrepancies in the observed growth of wind-generated waves, Journal of Physical Oceanography 22 (12) (1992) 1389–1405.

[66] O. Phillips, Spectral and statistical properties of the equilibrium range in wind-generated gravity waves, Journal of Fluid Mechanics 156 (1985) 505–531.

[67] S. Kitaigorodskii, On the theory of the equilibrium range in the spectrum of wind-generated gravity waves, Journal of Physical Oceanography 13 (5) (1983) 816–827.

[68] I. R. Young, Wind generated ocean waves, Vol. 2, Elsevier, 1999.

[69] Border lengths - states and territories.
URL http://www.ga.gov.au/scientific-topics/national-location-information/dimensions/

Electronic copy available at: https://ssrn.com/abstract=4758518

border-lengths

[70] Queensland governmet wave monitoring.
URL http://www.qld.gov.au/environment/coasts-waterways/beach/monitoring/

[71] K. Budal, J. Falnes, A resonant wave point absorber of ocean waves, Nature 256 (5517) (1975) 478–479.

[72] D. Evans, A theory for wave-power absorption by oscillating bodies, Journal of Fluid Mechanics 77 (1976) 1–25.

[73] J. V. Ringwood, S. Zhan, N. Faedo, Empowering wave energy with control technology: Possibilities and pitfalls, Annual Reviews in Control (2023).

[74] M. J. Tucker, E. G. Pitt, Waves in ocean engineering, no. Volume 5, Elsevier, 2001.

[75] C. Whittaker, A. Raby, C. Fitzgerald, P. Taylor, The average shape of large waves in the coastal zone, Coastal Engineering 114 (2016) 253–264.

Electronic copy available at: https://ssrn.com/abstract=4758518